Supplementary Information

S1 Supplementary Figures and Tables

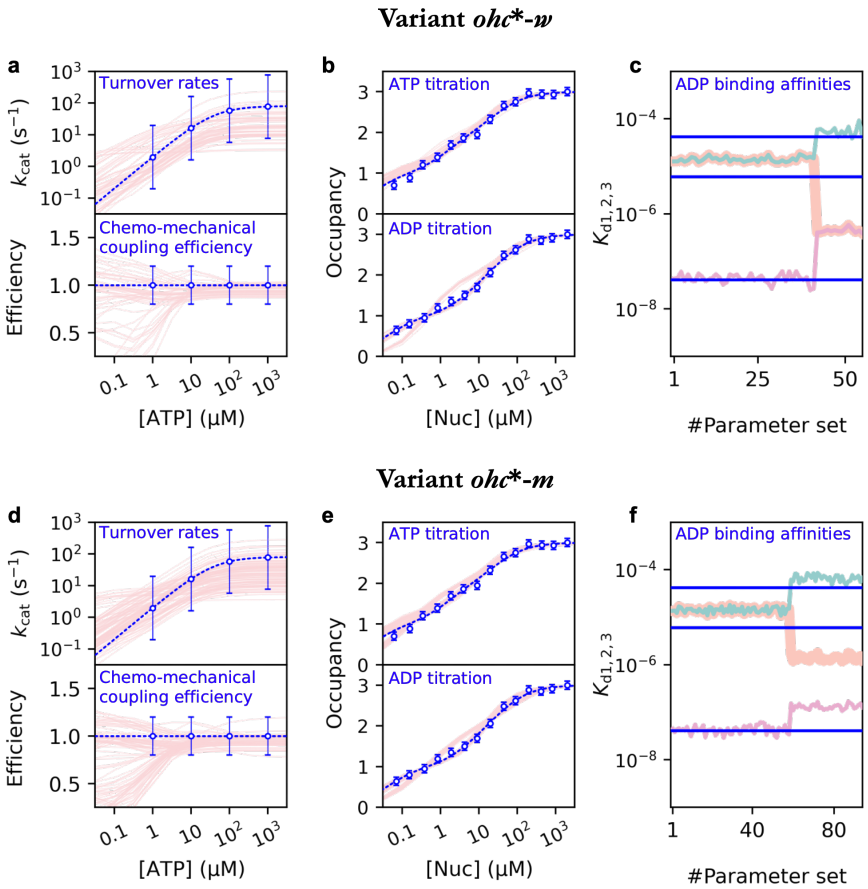

Fig. S1: **Predicted properties of variants *ohc*-w* and *ohc*-m* by the trained parameters**
a–**c**, **d**–**f** Predicted properties of variants *ohc*-w* and *ohc*-m* respectively. Representation consistent with Figure 2**a**–**c**.

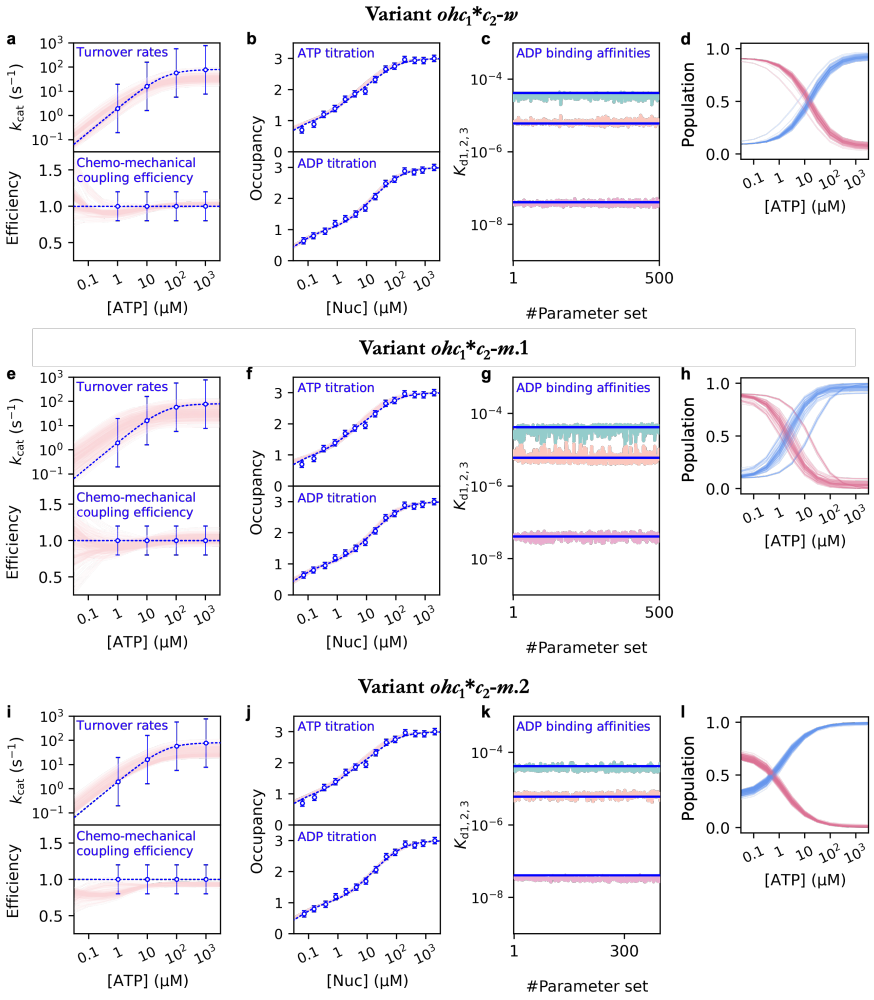

Fig. S2: **Predicted properties of variants** $ohc_1^*c_2$**-*w*, $ohc_1^*c_2$-*m*.1 and $ohc_1^*c_2$-*m*.2 by the trained parameters**

a–**d**, **e**–**h**, **i**–**l** Predicted properties of variants $ohc_1^*c_2$-*w*, $ohc_1^*c_2$-*m*.1 and $ohc_1^*c_2$-*m*.2 respectively.

a–**c**, **e**–**g**, **i**–**k** Representation consistent with Figure 2**a**–**c**.

d, **h**, **i** Predicted steady-state populations of the 80°- (blue curves) and 120-° states (dark pink curves).

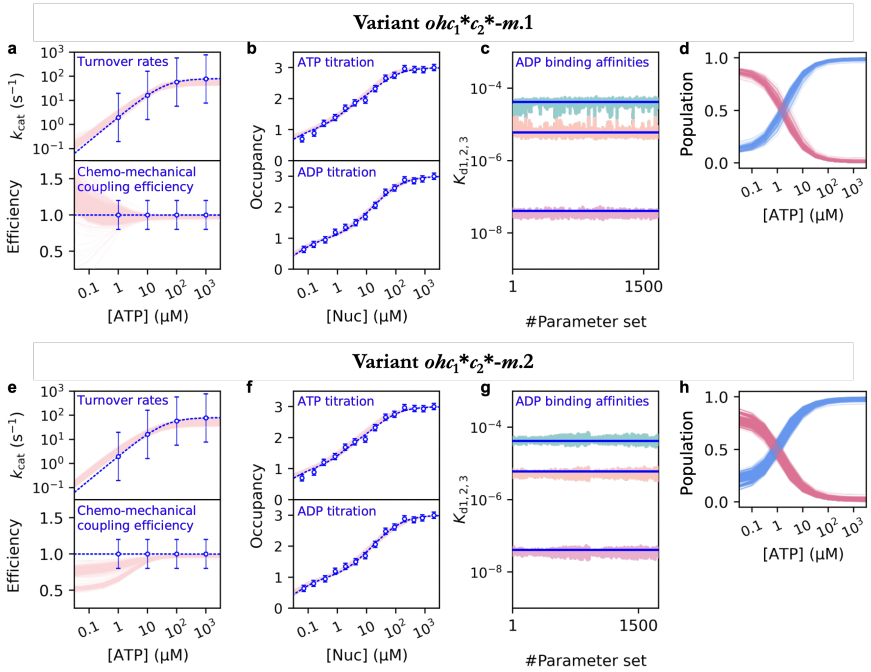

Fig. S3: Predicted properties of variants $ohc_1^*c_2^*$-*m*.1 and $ohc_1^*c_2^*$-*m*.2 by the trained parameters

a–**d**, **e**–**h** Predicted properties of variants $ohc_1^*c_2^*$-*m*.1 and $ohc_1^*c_2^*$-*m*.2 respectively.

a–**c**, **e**–**g** Representation consistent with Figure 2**a**–**c**.

d, **h** Predicted steady-state populations of the 80°- (blue curves) and 120-° states (dark pink curves).

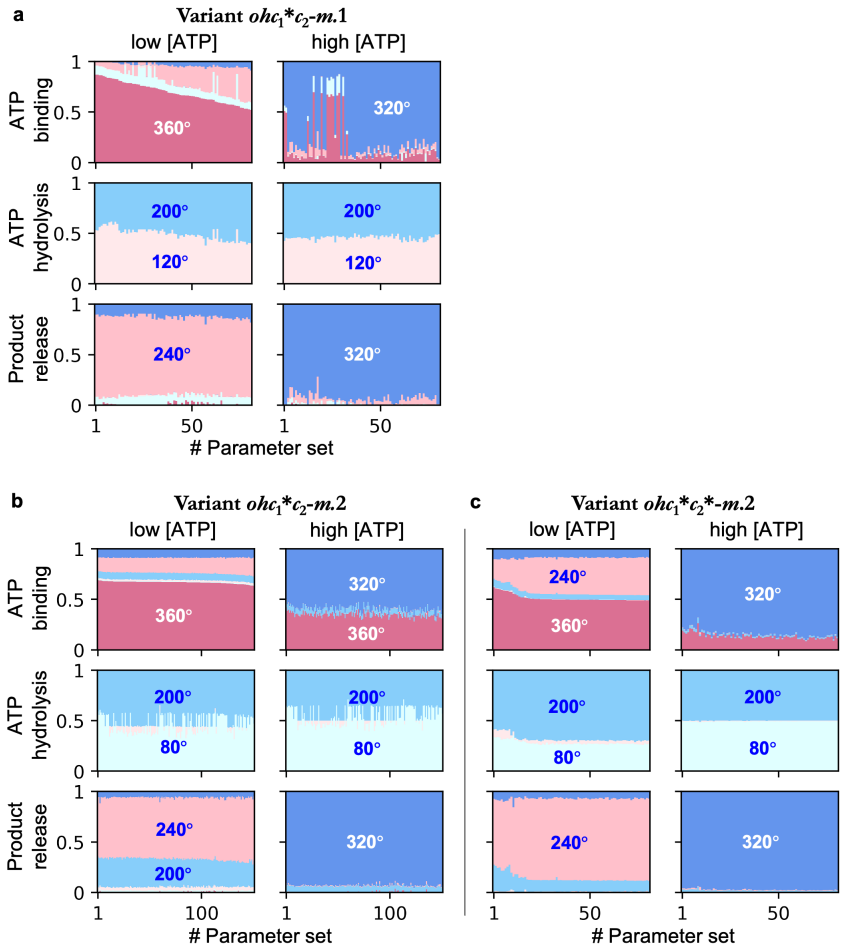

Fig. S4: Predicted probabilities of the major catalytic steps of the five tested ohc_1c_2-variants by the trained parameters
Representation consistent with Figure 2e.

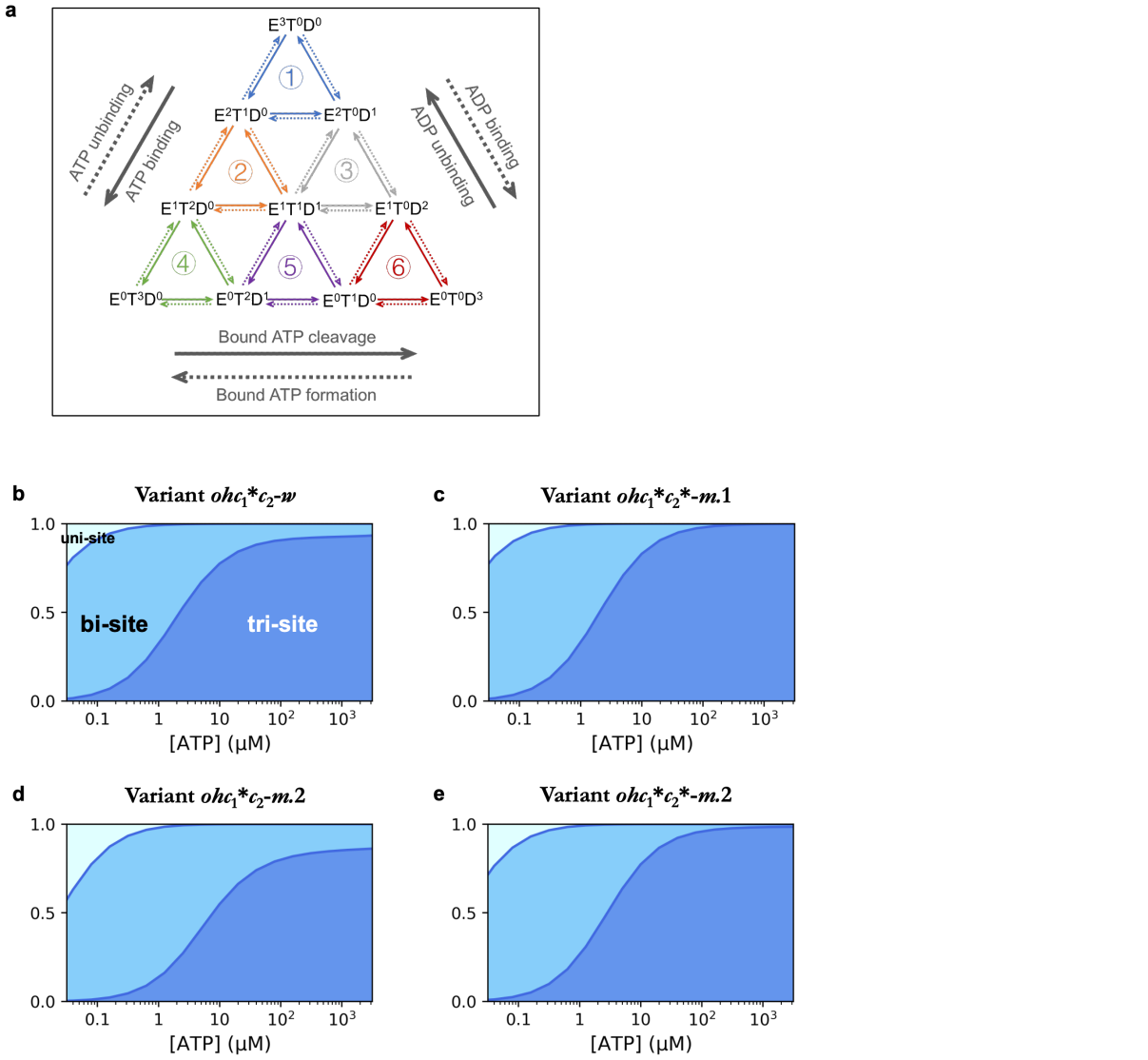

Fig. S5: Predicted contributions of uni-site, bi-site and tri-site pathways to the catalytic activity of F_1-ATPase

a Uni-site, bi-site and tri-site pathways. The Markov states are grouped by their chemical composition into 10 groups $\{E^xT^yD^z\}$, where x, y, z are integers from 0 to 3 and $x+y+z=3$. The states in group $E^xT^yD^z$ contains x empty catalytic site(s), y ATP-bound catalytic site(s), and z ADP-bound catalytic site(s). The arrows represent the transitions between the states, including ATP binding/unbinding, ADP binding/unbinding, and bound ATP hydrolysis/synthesis. Counterclockwise flow (solid arrows) and clockwise flow (dotted arrows) along a cycle (denoted in the figure by ①–⑥) corresponds to net ATP hydrolysis and synthesis, respectively. Cycle ① corresponds to uni-site pathways where the total nucleotide occupancy switches between zero and one; cycles ② and ③ correspond to bi-site pathways where the total nucleotide occupancy switches between one and two; cycles ④, ⑤ and ⑥ correspond to tri-site pathways where the total nucleotide occupancy switches between two and three.

b–**e** Predicted contributions of uni-site, bi-site and tri-site pathways to the catalytic activity of F_1-ATPase. Each panel shows for each variant the predictions by one parameter set randomly chosen from the trained parameter sets. The contribution of each pathway is defined as the ratio of the net hydrolysis rate along this pathway over the overall turnover rate, and shown in each panel by the height of the differently colored areas (light, medium and dark blue for uni-site, bi-site and tri-site pathways, respectively). For all the four variants, at physiological (millimolar) ATP concentration, tri-site pathways dominate the enzymatic activity (dark blue); at micromolar ATP concentration, bi-site pathways dominate instead (medium blue).

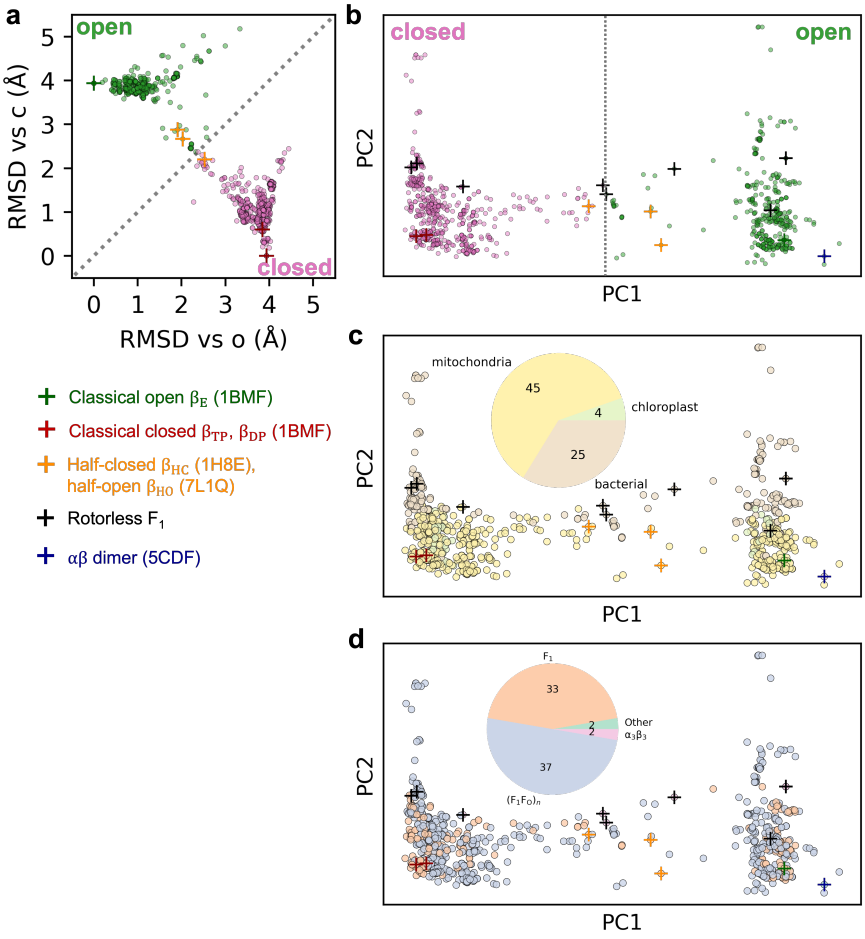

Fig. S6: **Summary and clustering of all β-subunits structures deposited into the Protein Data Bank**

We collected from the Protein Data Bank all the 331 structures containing β-subunit(s) that were determined in 74 studies. These 74 studies were classified into three categories according to the sources of the studied proteins (pie plot in **c**, mitochondria, chloroplast and bacteria), or four categories according to the composition of the studies protein (pie plot in **d**), including (1) an isolated β-subunit and a αβ dimer ("Other"), (2) several $\alpha_3\beta_3$ subcomplexes of F_1-ATPase ("$\alpha_3\beta_3$", also referred to as rotorless F_1), (3) several $\alpha_3\beta_3\gamma$ subcomplexes of F_1-ATPase and complete F_1-ATPase ("F_1"), as well as (4) monomers or multimers of F_1F_O-ATP synthase ("$(F_1F_O)_n$").
In total, 1077 β-subunit structures were extracted from these 331 structures for analysis illustrated by the scatter plots in panels **a**–**d**.
a RMSDs of the 1077 β-subunit structures compared to the classical open and closed conformations (β_E and β_{TP} from the crystal structure of PDB code 1BMF [4]). According to the RMSD versus the open conformation ($RMSD_o$, x-axis) and the RMSD versus the closed conformation ($RMSD_c$, y-axis), the 1077 structures were grouped into two clusters, denoted as open (green dots, $RMSD_o<RMSD_c$) and closed (pink dots, $RMSD_o>RMSD_c$).
b–**d** The 1077 β-subunit structures projected onto PC1 and PC2 (obtained from global principal component analysis), clustered according to RMSDs (**b**, consistent with **a**), source (**c**) or composition (**d**).

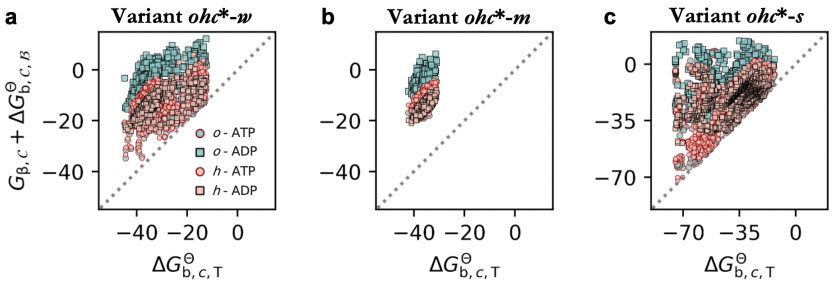

Fig. S7: **Comparing the free energies of a nucleotide-bound β-subunit adopting different conformations**
The free energies (in unit of $k_{\mathrm{B}}T$, assuming temperature $T = 298$ K) of an ATP/ADP-bound β-subunit adopting the o or h conformation ($G_{\beta,\mathcal{C}} + \Delta G^{\ominus}_{\mathrm{b},\mathcal{C},\mathcal{B}}$ for $\mathcal{C} = o, h$ and $\mathcal{B} = \mathrm{T}, \mathrm{D}$) compared to the that of an ATP-bound β-subunit adopting the c conformation ($\Delta G^{\ominus}_{\mathrm{b},c,\mathrm{T}}$). The gray dashed line represents the diagonal line above which $G_{\beta,\mathcal{C}} + \Delta G^{\ominus}_{\mathrm{b},\mathcal{C},\mathcal{B}} > \Delta G^{\ominus}_{\mathrm{b},c,\mathrm{T}}$.

Table S1: Dominant γ-orientations of the three major catalytic steps predicted by variant *ohc*-s*

Cluster	**ATP binding**		**ATP hydrolysis**	**Product release**	
	Low [ATP]	High [ATP]	Low and high [ATP]	Low [ATP]	High [ATP]
1	360° (0°)	240°, 320° (-120°, -40°)	120°(+120°)	120°, 200° (+120°, +200°)	200°, 320° (+200°, +320°)
2	360° (0°)	320° (-40°)	80°, 120° (+80°, +120°)	240°, 360° (+240°, +360°)	320° (+320°)
3	240°, 360°	320°	80°, 120°	240°, 360°	320°
4	200° (0°)	200° (0°)	80°, 120° (+240°, +280°)	240° (+400°)	240° (+400°)

S2 100% efficiency requires *c* to be the most stable conformation for a nucleotide-bound β-subunit

In the main article (Subsection 2.2), we have stated the conclusion that the *c* (closed and catalytically active) conformation being the most stable conformation for a nucleotide-bound β-subunit is a necessary condition for our model to reproduce the near 100% efficiency. Here, we present the evidence that leads us to this conclusion.

In Subsection 2.2, we have shown for variant *ohc-s* that all the trained parameter sets share the property that nucleotide-bound β-subunit has the lowest free energy when adopting the catalytically active, closed conformation *c* (Figure 2f). However, because the training data included in addition to the 100% efficiency also the measured ATP/ADP titration curves, it is not conclusive from Figure 2f alone whether this common property of the trained parameter sets is a requirement for our model to reproduce the 100% efficiency or the titration curves.

To address this question, we carried out a another round of training of variant *ohc-s* using our Bayesian approach (Methods), where only the experimental turnover rates and 100% efficiency were included as training data. Notably, the experimental turnover rates were still included in the training here to find meaningful parameter sets that predict effective rotary catalysis; otherwise, the training may be stuck in a region of the parameter space where hardly any catalysis or rotation is predicted, although the efficiency as a ratio of turnover and rotational rates could still be near 100%.

From the parameter sets found in this training we chose the sets that reproduce the experimental turnover rates and 100% efficiency. For these parameters, Supplementary Figure S7c shows the free energies of an ATP- or ADP-bound β-subunit adopting the *o* or *h* conformation ($G_{\beta,\mathcal{C}} + \Delta G^{\ominus}_{\mathrm{b},\mathcal{C},\mathcal{B}}$ for $\mathcal{C} = o, h$ and $\mathcal{B} = \mathrm{T}, \mathrm{D}$) against the free energy of an ATP-bound β-subunit adopting the *c* conformation ($\Delta G^{\ominus}_{\mathrm{b},c,\mathrm{T}}$). Similar to the previous observation (Figure 2f), here, all the parameter sets share the property that a nucleotide-bound β-subunit has the lowest free energy when adopting the catalytically active, closed conformation *c*.

Additionally, we also trained the other two investigated *ohc*-variants (variants *ohc-w* and *ohc-m*) against only the experimental turnover rates and 100% efficiency. Similar with variant *ohc-s*, parameter sets were found for both variants to reproduce these training data; all these parameter sets share the property

that a nucleotide-bound β-subunit has the lowest free energy when adopting the catalytically active, closed conformation c (Supplementary Figure S7a, b).

These results provide strong evidence for our conclusion that the c conformation being the most stable conformation for a nucleotide-bound β-subunit is a necessary condition for our model to reproduce the near 100% efficiency. This condition is mathematically expressed by

$$G_{\beta,\mathcal{C}} + \Delta G^{\ominus}_{\mathrm{b},\mathcal{C},\mathcal{B}} > \Delta G^{\ominus}_{\mathrm{b},c,\mathrm{T}} \tag{S2.1}$$

for $\mathcal{C} = o, h$ and $\mathcal{B} = \mathrm{T}, \mathrm{D}$. In the main article (Subsection 2.2), we have also provided a plausible explanation for this condition.

Most importantly, this condition is not restricted to a specific variant of our model; given the plausible explanation, we suggest that it is highly likely a general conclusion depending only on the very basic assumptions of our model (Subsection 2.1) which are actually common notions about F_1-ATPase. Therefore, we suggest that c being the most stable conformation is not only the mechanism by which our model reproduces the near 100 %efficiency, but also the way in which F_1-ATPases have evolved to maintain the tight chemo-mechanical coupling between ATP hydrolysis within the β-subunits and the rotation of the γ-subunit under a wide range of ATP concentrations.

S3 Observed γ-orientations of the three major catalytic steps

Here, we summarize a series of single-molecule experiments that are intended to determine the γ-subunit orientations at which the three major catalytic steps in a β-subunit occur, namely, ATP binding, ATP hydrolysis and the rate-limiting product release. As explained at the end of this section, these summarized observations, in retrospect, lead to a deterministic model that assigns each catalytic step to a particular γ-orientation; we used this deterministic model as validation data to evaluate our Markov model.

A brief review of the single-molecule observations The major technique employed in the single-molecule experiments on F_1-ATPase is fluorescence microscopy imaging, which allows direct visualization of the rotation of the γ-subunit. An $\alpha_3\beta_3\gamma$ subcomplex of F_1-ATPase derived from the thermophilic *Bacillus PS3* with several mutations was used. These mutations include α-C193S and an extra his-tag (consisted of ten histidines) at the amino terminus of each β-subunit to immobilize the stator $\alpha_3\beta_3$ onto a surface, as well as γ-S107C and γ-I210C to attach a colloidal gold or magnetic bead to the γ-subunit via a biotin-streptavidin-BSA linker [8, 13, 14]. The bead was imaged under fluorescence microscopy to record a time trace of its orientation; the orientation of the bead is supposed to closely follow the orientation of the γ-subunit [8, 15, 25, 34, 47].

R. Yasuda *et al.* first resolved the 90°- and 30°-substeps of γ-subunit rotation from such time traces of bead orientations [8]. These traces show two dwells before and after the 30°-substeps, which are termed the 90°- and 120°-dwell respectively. At low ATP concentrations (0.2 μM and below), the 120°-dwell is dominant while the 90°-dwell is hardly seen. The 120°-dwell becomes longer with decreasing ATP concentration; the distribution of the duration is fitted by a single exponential function $f(t) \propto \exp(-k_1 t)$, where the rate k_1 is dependent on ATP concentration, $k_1 \approx (3 \times 10^7\,\mathrm{s}^{-1}\cdot\mathrm{M}^{-1}) \times [\mathrm{ATP}]$. It was therefore hypothesized that the 120°-dwell is limited by ATP binding to an *apo* β-subunit (ATP-waiting dwell), and the ATP binding rate coefficient is estimated to be $3 \times 10^7\,\mathrm{s}^{-1}\cdot\mathrm{M}^{-1}$. At high ATP concentrations (60 μM and above), the 90°-dwell becomes dominant while the 120°-dwell is hardly seen. The distribution of the duration of the 90°-dwell is fitted by a double exponential function $f(t) \propto \exp(-k_2 t) - \exp(-k_3 t)$, where the two rates $k_2 = (0.71 \pm 0.02)\,\mathrm{ms}^{-1}$ and $k_3 = (1.64 \pm 0.06)\,\mathrm{ms}^{-1}$ do not depend on ATP concentration ([ATP]). It was therefore hypothesized that the 90°-dwell is limited by two ∼1 ms reactions, which may be, *e.g.*, ATP hydrolysis and product release. The 90°-dwell is thus termed the catalytic dwell. At intermediate ATP

concentrations (2 μM – 20 μM), both dwells are seen, and the distributions of the dwell times are compatible with the three rate limiting steps of rates k_1 ([ATP]-dependent), k_2 and k_3 ([ATP]-independent).

The two ∼1 ms reactions limiting the catalytic dwell are suggested to be ATP hydrolysis and phosphate release, respectively. First, K. Shimabukuro *et al.* [47] introduced an extra mutation β-E190D into each of the three β-subunits; this mutation had been shown to remarkably slow down ATP hydrolysis. Additionally, they used a slowly hydrolysable ATP analog ATPγS instead of ATP as substrate. As a result, they observed significant elongation of the catalytic dwell, which suggests that ATP hydrolysis is a rate limiting step of the catalytic dwell, and may correspond to one of the two ∼1 ms reactions observed in [8]. Additionally, this study refined the previously reported 90°- and 30°-substeps [8] to be 80° and 40° instead, still within the previously estimated errorbar [8], giving rise to the notions of catalytic dwell around 80° and ATP-waiting dwell around 120° [15, 26, 34].

Further, to determine the exact γ-orientations of ATP hydrolysis in a β-subunit, T. Ariga *et al.* [26] visualized the rotation of hybrid $\alpha_3\beta_3\gamma$ constructs containing one or two β-subunits with mutation β-E190D. The observed time traces of the bead orientations show that in a mutant β-subunit, the catalytic dwell at +200° relative to ATP binding is remarkably elongated, suggesting that ATP hydrolysis in this β-subunit limits the rotation from +200° to +240°. Additionally, the catalytic dwell at +320° is also elongated, suggesting a third catalytic event (∼20 ms) in this β-subunit limiting the rotation from +320° to +360°. However, this study did not determine what this third catalytic event represents.

Second, K. Adachi *et al.* [15] observed that the catalytic dwell is also remarkably elongated when an excessive amount of phosphate is added into the buffer. This observation suggests that the other ∼1 ms reaction within the catalytic dwell is likely phosphate release. Naïvely, phosphate concentration in the buffer does not directly affect the rate of phosphate release; however, as suggested by the authors, high phosphate concentration results in frequent phosphate rebinding, which in turn results in reversal of the +40°-substep and thus elongation of the catalytic dwell.

Combining the conclusions of Refs. [26] and [15], R. Watanabe *et al.* [34] suggested that the third catalytic event observed for the hybrid F_1-ATPase constructs at +320° [26] actually represents phosphate release. Using high concentration (1 mM) of ATPγS as substrate, they arrested the γ-subunit within

a catalytic dwell for a while using magnetic tweezers; then, they released the γ-subunit and observed whether it proceeded forward to the next catalytic angle or stayed at the stalled angle. They observed these two behaviors of similar frequencies, which suggested that ATP hydrolysis remains reversible at +200°. Because the reversibility of ATP hydrolysis requires the presence of phosphate still in the catalytic site, this study provides evidence for phosphate release later than +200° at high ATP concentration. Considering the conclusion from Ref. [15] that phosphate release occurs within a catalytic dwell, the authors concluded that phosphate release occurs at +320°.

Besides ATP binding, ATP hydrolysis, and phosphate release, one would expect the release of the other product, *i.e.*, ADP, to also be a major catalytic step. Unexpectedly, evidences have been reported showing that ADP release is a very fast reaction within the ATP-waiting dwell under room temperature, and occurs between +240° and +320°, earlier than phosphate release [15, 25, 48, 49].

Discussion about the single-molecule data and our deterministic model In summary of the above observations, Watanabe *et al.* proposed a deterministic model for the γ-orientations of the major catalytic steps, to which we refer as the Watanabe model (see particularly Figure 6 in Ref. [34]). At low [ATP], ATP binding in a β-subunit occurs in a 120°-dwell, and this γ-orientation is taken as 0°. In this very β-subunit, the bound ATP is hydrolyzed at +200°; the product ADP is released at +240°, but this reaction is too fast to be observed under room temperature; finally, the other product, phosphate, is released at +320°. At high [ATP], ATP binding may occur immediately after phosphate release at +320°.

We note that several statements in the Watanabe model remain controversial. Below, we attempt to propose a more general and inclusive model that reconciles these controversies and aligns with other experimental data as well as theoretical insights.

First, the γ-orientations of ADP and phosphate release have been debated in the publications. The opposite opinion argues that phosphate release is fast and precedes ADP release. The crystal and cryoEM structures of F_1-ATPase often capture states containing ADP- or ADP+Pi-bound β-subunits [4, 5, 24], and only in rare cases are β-subunits bound with only phosphate or phosphate analogs observed [24, 68]. The higher chance to observe ADP- and ADP+Pi-bound states than to observe Pi-bound states indicates that ADP is likely to linger in the catalytic site longer than phosphate. Additionally, it has been reported that ADP has a much higher binding affinity with the β-subunits than phosphate [54],

which renders it physically implausible that phosphate release is a rate-limiting step whereas ADP release is not.

Another evidence against late and slow phosphate release is that under saturating ATP concentration, the total nucleotide occupancy approaches three [20–22]. If ADP were released as early as +240° whereas phosphate remained in the catalytic site until +320°, and if phosphate release were also a rate-limiting step of the catalytic dwell taking about 1 ms [8], the total nucleotide occupancy would be substantially below three, contradicting the measured occupancy. A possible fix is that phosphate release is actually a fast reaction and occurs at the beginning of the +320° [34].

In all, it is unlikely that phosphate release is both slower and later than ADP release. The remaining possibilities are: (1) ADP release is a rate-limiting step of the +320°-dwell, while phosphate release is a fast reaction; (2) phosphate release is a rate-limiting step of the +320°-dwell while ADP release is a fast reaction, but ADP lingers in the catalytic site longer. Considering both possibilities, we assume in our deterministic model that there is only one product release step that is rate-limiting, either ADP release or phosphate release, and this rate-limiting product release step occurs at at +320° (Results and Discussion).

Second, we note that, according to the above experimental data alone, the possibility cannot be ruled out that under low ATP concentration, the rate-limiting product release step occurs at γ-orientations other than +320°. In fact, under low ATP concentrations, the 80°-dwells are much shorter than the 120°-dwells and therefore hardly recognized in the recorded trajectories. Therefore, our deterministic model only assumes that the rate-limiting product release step occurs at +320° under high ATP concentration, but allows for variations under low ATP concentration.

Third, the hypothesis in Watanabe model that ATP hydrolysis occurs at +200° is also questionable. As already explained, this hypothesis is based on the observation of a mutant F_1-ATPase hydrolyzing an ATP analog where hydrolysis is drastically slowed down [26]. For native F_1-ATPase and substrate, ATP hydrolysis might occur at γ-orientations earlier than +200°, but not later. Accordingly, we assume in our deterministic model that ATP hydrolysis occurs no later than +200°.

In summary, our deterministic model is formulated as following: ATP binding in a β-subunit under low ATP concentration occurs within a 120°-dwell; denoting

the γ-orientation at which ATP binding in β_3 occurs as 360° (0°), the bound ATP is hydrolyzed no later than +200°, and the rate-limiting product release occurs under high ATP concentration at +320°.

S4 Reducing the choices of γ-β restrictions via physical constraints

Here, we detail our analysis on physics grounds about the conditions the γ-β restrictions must meet for a variant of our generic Markov model to reproduce the experimental data, including particularly the observed γ-orientations of the major catalytic steps. This analysis helps reduce the huge hyperparameter space of γ-β restrictions.

For clarity, below we will use some formal notations for the γ-β restrictions. Due to the three-fold rotational pseudo-symmetry of the F_1-ATPase structure, specifying six Γ_k^ϕ, *e.g.*, $\{\Gamma_k^\phi | k = 1, 2, 3; \phi = 80°, 120°\}$ (denoted as $\{\Gamma_{1,2,3}^{80°,120°}\}$) or $\{\Gamma_3^\phi | \phi = 360°, 80°, 120°, 200°, 240°, 320°\}$ (denoted as $\{\Gamma_3^\phi\}$), is sufficient to uniquely determine a specific variant. These two sets of six Γ_k^ϕ are equivalent via

$$\Gamma_1^{80°} = \Gamma_3^{320°}, \Gamma_1^{120°} = \Gamma_3^{360°} (\equiv \Gamma_3^{0°}), \Gamma_2^{80°} = \Gamma_3^{200°}, \Gamma_2^{120°} = \Gamma_3^{240°}. \tag{S4.1}$$

The other Γ_k^ϕ, knowing $\{\Gamma_3^\phi\}$, are determined by

$$\Gamma_1^\phi = \Gamma_3^{\mathrm{mod}(\phi+240°,360°)}, \Gamma_2^\phi = \Gamma_3^{\mathrm{mod}(\phi+120°,360°)}, \tag{S4.2}$$

for $\phi = 360°, 80°, 120°, 200°, 240°, 320°$, where $\mathrm{mod}(x, y)$ represents the modulus of x divided by y.

The observed γ-orientations of the major catalytic steps include: (1) under low ATP concentration, ATP binds to an empty β-subunit within a 120°-dwell; starting from this orientation (0°), in this very β-subunit and under high ATP concentration, (2) hydrolysis of the bound ATP occurs no later than +200°; (3) the rate-limiting product release occurs at +320°. These observations apply to any of the three β-subunits. For clarity, below we will focus on β_3, and, without losing generality, stipulate that ATP binding occurs in β_3 at the γ-orientation of 360° (Figure 1c), so that ATP hydrolysis and product release occur at the γ-orientations of 200° and 320°, respectively. Accordingly, we will first focus on determining the conditions of $\{\Gamma_3^\phi\}$, and then convert them to $\{\Gamma_{1,2,3}^{80°,120°}\}$ to provide a compact denotation in the form of a table (see Table S9 for example).

Our analysis starts from the important finding (Subsection 2.2) that the free energy of a nucleotide-bound β-subunit is lower when it adopts the catalytically active closed conformation c than when it adopts the open or partially open conformations o and h, *i.e.*, a nucleotide-bound β-subunit remains closed unless restricted to the o and h conformations by the γ-subunit. This is shown to be

the fundamental condition for our model to reproduce the observed near 100% chemo-mechanical coupling efficiency of F_1-ATPase (Supplementary Section S2).

Following this condition, two conditions of the γ-β restrictions to reproduce the observed orientations of major catalytic steps can be directly implied: first, for ATP hydrolysis to occur at 200°, $\Gamma_3^{200^\circ}$ must include at least one catalytically active conformation; second, for ATP binding and product release to occur at 360°and 320°respectively, $\Gamma_3^{360^\circ}$ and $\Gamma_3^{320^\circ}$ must exclude any closed conformation so that β_3 adopts the conformation o or h where nucleotide exchange is likely, *i.e.*, $\Gamma_3^{360^\circ}$ and $\Gamma_3^{320^\circ}$ can be $\{o\}$ or $\{o, h\}$. Here, note that we have already assumed that $\Gamma_3^{360^\circ}$=$\{o\}$ following previous studies [5, 22, 23].

Our analysis is further developed from this condition by considering the fundamental idea of "binding change" [6, 16, 52], which states that a catalytic step in a β-subunit is induced by the conformational transition of the β-subunit, and that the latter is coupled to the rotation of the γ-subunit. Thus, observing a catalytic step at an orientation implies certain conformational transition of the β-subunit at this orientation that would induce this change of binding state. For example, observing ATP hydrolysis in β_3 at 200° implies that β_3 converts from a catalytically active conformation to an inactive conformation as the γ-subunit rotates from 200° to 240°, and this conformational transition must be allowed for and enforced in our model by proper choices of $\Gamma_3^{200^\circ}$ and $\Gamma_3^{240^\circ}$. Specifically, at 200°, β_3 must be allowed to adopt a catalytically active conformation where reversible ATP hydrolysis takes place; further, as the γ-subunit proceeds to 240°, β_3 must be restricted from any catalytically active conformation so that ATP is irreversibly converted to product.

Exclusion of ohc-variants based on observed orientations of major catalytic steps

For *ohc*-variants, Γ_3^ϕ have three options, $\{o\}$, $\{o, h\}$, or $\{o, h, c\}$. Because only the c conformation is catalytically active, following the previous arguments, $\Gamma_3^{200^\circ}$ must be $\{o, h, c\}$ and $\Gamma_3^{240^\circ}$ can be $\{o\}$ or $\{o, h\}$. Along similar lines, the conditions of γ-β restrictionsto reproduce the observed γ-orientations of ATP binding and product release can also be inferred. In particular, we state that Γ_3^ϕ must change at the observed γ-orientations of the major catalytic steps as the γ-subunit rotates further counterclockwise, *i.e.*, $\Gamma_3^{360^\circ} \neq \Gamma_3^{80^\circ}$, $\Gamma_3^{200^\circ} \neq \Gamma_3^{240^\circ}$ and $\Gamma_3^{320^\circ} \neq \Gamma_3^{360^\circ}$. Only by the change of Γ_3^ϕ is it possible for β_3 to undergo proper conformational changes at these orientations that lead to the corresponding catalytic steps.

Accordingly, in β_3:

(1) For product release to occur at 320°, recalling our assumption that $\Gamma_3^{360°} = \{o\}$ and the previously found condition that $\Gamma_3^{320°} = \{o\}$ or $\{o, h\}$, $\Gamma_3^{320°}$ can only be $\{o, h\}$. β_3 is expected to preferably adopt the h conformation at 320°, release the product and then opens up completely. It is therefore known that conformational transition from h to o induces product release. This further implies that $\Gamma_3^{240°}$ can only be $\{o, h\}$, otherwise (*i.e.*, if $\Gamma_3^{240°} = \{o\}$) product release would occur at 200° already.

(2) For ATP binding to occur at 360° (0°), $\Gamma_3^{80°}$ must be different from $\Gamma_3^{360°} = \{o\}$, therefore $\Gamma_3^{80°}$ can be $\{o, h\}$ or $\{o, h, c\}$.

Finally, between 80° and 200°, β_3 should be allowed to close completely at some orientation and remain closed afterwards until ATP hydrolysis at 200°. Therefore, there are three possible combinations of $\Gamma_3^{80°}$ and $\Gamma_3^{120°}$: i. $\Gamma_3^{80°} = \Gamma_3^{120°} = \{o, h, c\}$; ii. $\Gamma_3^{80°} = \{o, h\}$, $\Gamma_3^{120°} = \{o, h, c\}$; and iii. $\Gamma_3^{80°} = \Gamma_3^{120°} = \{o, h\}$.

In conclusion, we have reduced the rather large hyperparameter space of the γ-β restrictions (3^5–$2^5 = 221$ *ohc*-variants, where the subtraction excludes the 2^5 variants where c is completely missing) to only three variants that would potentially reproduce the observed γ-orientations of the major catalytic steps.

However, none of these three variants explains all available experimental data. Combination i of $\Gamma_3^{80°}$ and $\Gamma_3^{120°}$ results in variant *ohc-m*, which has been shown in Subsection 2.2 to disagree with the measured binding affinities. Combinations ii and iii restricts β_3 from adopting the c conformation at 80°. The resultant variants would predict at most one closed β-subunit at any γ-orientation. This prediction disagrees with the determined crystal and cryoEM structures of F_1-ATPase where two β-subunits adopt similar closed conformations at 80° and/or 120° [4, 5, 24].

Therefore, we conclude that no *ohc**-variant would explain all available experimental data, and we are forced to include at least four β-subunit conformations within our model.

Definition of ohc$_1$c$_2$-variants One option is to include an additional closed conformation, considering the notion that the two closed β-subunits in the classic crystal structure [4], β_{TP} and β_{DP}, are different [4, 5, 55]. The resultant two closed conformations will be referred to as c_1 and c_2, tentatively associated with β_{TP} and β_{DP}, respectively. Accordingly, each Γ_3^{ϕ} has five options, $\{o\}$, $\{o, h\}$, $\{o, h, c_1\}$, $\{o, h, c_2\}$ and $\{o, h, c_1, c_2\}$. The catalytically active conformation(s) may include c_1 only (*ohc*$_1^*$c$_2$-variants) or both c_1 and c_2 (*ohc*$_1^*$c$_2^*$-variants). We also

assumed that a β-subunit can directly convert between c_1 and c_2. The assumption also imposes conditions some conditions on γ-β restrictions, which will be discussed later.

Exclusion of ohc_1c_2-variants based on observed orientations of major catalytic steps

Following similar arguments by which we found conditions of the γ-β restrictions for the *ohc*-variants to reproduce the observed orientations of the major catalytic steps, we next analyze conditions for the ohc_1c_2-variants.

For ATP hydrolysis to occur at 200°, $\Gamma_3^{200^\circ}$ can be $\{o,h,c_1\}$, $\{o,h,c_2\}$ (only for $ohc_1^*c_2^*$-variants) or $\{o,h,c_1,c_2\}$, allowing β_3 to adopt at least one catalytically active conformation at 200°; $\Gamma_3^{240^\circ}$ can be $\{o\}$, $\{o,h\}$ or $\{o,h,c_2\}$ (only for $ohc_1^*c_2$-variants), restricting β_3 from any catalytically active conformation at 240°. For $ohc_1^*c_2^*$-variants, because c_1 and c_2 are completely equivalent, we ask $\Gamma_3^{200^\circ}$ to necessarily include c_1 without losing generality, *i.e.*, $\Gamma_3^{200^\circ} = \{o,h,c_1\}$ or $\{o,h,c_1,c_2\}$.

For product release to occur at 320°, $\Gamma_3^{320^\circ} = \{o,h\}$. Additionally, $\Gamma_3^{240^\circ}$ can only be $\{o,h\}$ or $\{o,h,c_2\}$ (only for $ohc_1^*c_2$-variants), otherwise (*i.e.*, if $\Gamma_3^{240^\circ} = \{o\}$) product release would occur at 200° already.

For ATP binding to occur at 360°, $\Gamma_3^{80^\circ}$ must be different from $\Gamma_3^{360^\circ} = \{o\}$, hence can be $\{o,h\}$, $\{o,h,c_1\}$, $\{o,h,c_2\}$ or $\{o,h,c_1,c_2\}$. Between 80° and 200°, β_3 should be allowed to close completely at some orientation and remain closed afterwards until ATP hydrolysis at 200°. Therefore, the possible combinations of $\Gamma_3^{80^\circ}$ and $\Gamma_3^{120^\circ}$ are:

(1) If $\Gamma_3^{80^\circ} = \{o,h\}$, then $\Gamma_3^{120^\circ} = \{o,h\}$, $\{o,h,c_1\}$, $\{o,h,c_2\}$ or $\{o,h,c_1,c_2\}$;

(2) If $\Gamma_3^{80^\circ} = \{o,h,c_1\}$, then $\Gamma_3^{120^\circ} = \{o,h,c_1\}$ or $\{o,h,c_1,c_2\}$;

(3) If $\Gamma_3^{80^\circ} = \{o,h,c_2\}$, then $\Gamma_3^{120^\circ} = \{o,h,c_1\}$ (only for $ohc_1^*c_2$-variants), $\{o,h,c_2\}$ or $\{o,h,c_1,c_2\}$;

(4) If $\Gamma_3^{80^\circ} = \{o,h,c_1,c_2\}$, then $\Gamma_3^{120^\circ} = \{o,h,c_1\}$, $\{o,h,c_2\}$ (only for $ohc_1^*c_2^*$-variants) or $\{o,h,c_1,c_2\}$.

Besides $\Gamma_1^{120^\circ} = \{o\}$, these found conditions of $\{\Gamma_3^\phi\}$ converts to $\{\Gamma_{1,2,3}^{80^\circ,120^\circ}\}$: $\Gamma_1^{80^\circ} = \{o,h\}$, $\Gamma_2^{80^\circ} = \{o,h,c_1\}$ or $\{o,h,c_1,c_2\}$, $\Gamma_2^{120^\circ} = \{o,h\}$ or $\{o,h,c_2\}$ (only for $ohc_1^*c_2$-variants), and the possible combinations of $\Gamma_3^{80^\circ}$ and $\Gamma_3^{120^\circ}$ as stated above. Counting the possible combinations of $\{\Gamma_{1,2,3}^{80^\circ,120^\circ}\}$, there are $2\times1\times(4+2+2+3) =$

22 $ohc_1^*c_2^*$-variants and $2 \times 2 \times (4 + 2 + 3 + 2) = 44$ $ohc_1^*c_2$-variants. This is, however, still a large number of variants.

Further exclusion of ohc_1c_2-variants Therefore, we further excluded some of these ohc_1c_2-variants based on a recent tryptophan fluorescence experiment [22]. This experiment measured the ADP titration curves of F_1-ATPase stalled in the 80°- and 120°-dwells; each of these titration curves shows three distinct binding affinities, suggesting that the three β-subunits are differentiated in both the 80°- and 120°-dwells. According to the analytical expressions of the binding affinities we derived in Supplementary Section S5 (see particularly Equation (S5.22)), for our model to agree with this study, the γ-β restrictions must be different for the three β-subunits for at 80° and 120°, *i.e.*, $\Gamma_1^\phi \neq \Gamma_2^\phi$, $\Gamma_1^\phi \neq \Gamma_3^\phi$ and $\Gamma_2^\phi \neq \Gamma_3^\phi$ for $\phi = 80°$, 120°.

Accordingly, the possible combinations of $\Gamma_2^{80°}$, $\Gamma_3^{80°}$, $\Gamma_2^{120°}$ and $\Gamma_3^{120°}$ are reduced to those shown in Tables S2 (for $ohc_1^*c_2^*$-variants), S3 (for $ohc_1^*c_2$-variants assuming $\Gamma_2^{120°} = \{o, h\}$) and S4 (for $ohc_1^*c_2$-variants assuming $\Gamma_2^{120°} = \{o, h, c_2\}$). Accordingly, there are 9 $ohc_1^*c_2^*$-variants and 18 $ohc_1^*c_2$-variants left.

Table S2: The remaining possible combinations of γ-β restrictions for $ohc_1^*c_2^*$-variants after considering the differentiated binding affinities

$\Gamma_2^{80°}$	$\Gamma_3^{80°}$	$\Gamma_3^{120°}$	Count
$\{o, h, c_1\}$	$\{o, h, c_2\}$	$\{o, h, c_2\}$ or $\{o, h, c_1, c_2\}$	2
	$\{o, h, c_1, c_2\}$	$\{o, h, c_1\}$, $\{o, h, c_2\}$ or $\{o, h, c_1, c_2\}$	3
$\{o, h, c_1, c_2\}$	$\{o, h, c_1\}$	$\{o, h, c_1\}$ or $\{o, h, c_1, c_2\}$	2
	$\{o, h, c_2\}$	$\{o, h, c_2\}$ or $\{o, h, c_1, c_2\}$	2

Table S3: The remaining possible combinations of γ-β restrictions for $ohc_1^*c_2$-variants with $\Gamma_2^{120°} = \{o, h\}$ after considering the differentiated binding affinities

$\Gamma_2^{80°}$	$\Gamma_3^{80°}$	$\Gamma_3^{120°}$	Count
$\{o, h, c_1\}$	$\{o, h, c_2\}$	$\{o, h, c_1\}$, $\{o, h, c_2\}$ or $\{o, h, c_1, c_2\}$	3
	$\{o, h, c_1, c_2\}$	$\{o, h, c_1\}$ or $\{o, h, c_1, c_2\}$	2
$\{o, h, c_1, c_2\}$	$\{o, h, c_1\}$	$\{o, h, c_1\}$ or $\{o, h, c_1, c_2\}$	2
	$\{o, h, c_2\}$	$\{o, h, c_1\}$, $\{o, h, c_2\}$ or $\{o, h, c_1, c_2\}$	3

Table S4: The remaining possible combinations of γ-β restrictions for $ohc_1^*c_2$-variants with $\Gamma_2^{120^\circ} = \{o, h, c_2\}$ after considering the differentiated binding affinities

$\Gamma_2^{80^\circ}$	$\Gamma_3^{80^\circ}$	$\Gamma_3^{120^\circ}$	Count
$\{o, h, c_1\}$	$\{o, h, c_2\}$	$\{o, h, c_1\}$ or $\{o, h, c_1, c_2\}$	2
	$\{o, h, c_1, c_2\}$	$\{o, h, c_1\}$ or $\{o, h, c_1, c_2\}$	2
$\{o, h, c_1, c_2\}$	$\{o, h, c_1\}$	$\{o, h, c_1\}$ or $\{o, h, c_1, c_2\}$	2
	$\{o, h, c_2\}$	$\{o, h, c_1\}$ or $\{o, h, c_1, c_2\}$	2

Finally, we note that only 15 out of these 27 ohc_1c_2-variants are compatible with our assumption that a β-subunit can directly convert between c_1 and c_2. For these 15 variants, Γ_3^{ϕ} at every two adjacent orientations (*i.e.*, $\Gamma_3^{80^\circ}$ and $\Gamma_3^{120^\circ}$, $\Gamma_3^{120^\circ}$ and $\Gamma_3^{200^\circ} \equiv \Gamma_2^{80^\circ}$) include at least one same closed conformation. This condition allows β_3 to convert between c_1 and c_2 directly, without opening (partially) first and closing again ($c_1/c_2 \rightarrow h \rightarrow c_1/c_2$).

These 15 ohc_1c_2-variants include 5 $ohc_1^*c_2^*$-variants and 10 $ohc_1^*c_2$-variants. Their combinations of $\Gamma_2^{80^\circ}$, $\Gamma_3^{80^\circ}$, $\Gamma_2^{120^\circ}$ and $\Gamma_3^{120^\circ}$ are shown in Tables S5 (for $ohc_1^*c_2^*$-variants), S6 (for $ohc_1^*c_2$-variants assuming $\Gamma_2^{120^\circ} = \{o, h\}$) and S7 (for $ohc_1^*c_2$-variants assuming $\Gamma_2^{120^\circ} = \{o, h, c_2\}$). Notably, two $ohc_1^*c_2^*$-variants are omitted (last row in Table S5, where $\Gamma_2^{80^\circ}$=$\{o, h, c_1, c_2\}$, $\Gamma_3^{80^\circ}$=$\{o, h, c_2\}$), because they are equivalent to the other two $ohc_1^*c_2^*$-variants (fourth row in Table S5, where $\Gamma_2^{80^\circ}$=$\{o, h, c_1, c_2\}$, $\Gamma_3^{80^\circ}$=$\{o, h, c_1\}$) considering the equivalence of the c_1 and c_2 conformations.

Table S5: The finally remaining possible combinations of γ-β restrictions for $ohc_1^*c_2^*$-variants

$\Gamma_2^{80^\circ}$	$\Gamma_3^{80^\circ}$	$\Gamma_3^{120^\circ}$	Count
$\{o, h, c_1\}$	$\{o, h, c_2\}$	$\{o, h, c_1, c_2\}$	1
	$\{o, h, c_1, c_2\}$	$\{o, h, c_1\}$ or $\{o, h, c_1, c_2\}$	2
$\{o, h, c_1, c_2\}$	$\{o, h, c_1\}$	$\{o, h, c_1\}$ or $\{o, h, c_1, c_2\}$	2
	$\{o, h, c_2\}$	$\{o, h, c_2\}$ or $\{o, h, c_1, c_2\}$	--

Search for the minimal ohc_1c_2-variants We classified these 15 ohc_1c_2-variants into five groups (Table S8) according to the number of Markov states included in each variant. From group 1 to 5, the number of included Markov states decreases from 972 to 702. We consider the variants including less Markov states more

Table S6: The finally remaining possible combinations of γ-β restrictions for $ohc_1^*c_2$-variants with $\Gamma_2^{120^\circ} = \{o, h\}$

$\Gamma_2^{80^\circ}$	$\Gamma_3^{80^\circ}$	$\Gamma_3^{120^\circ}$	Count
$\{o, h, c_1\}$	$\{o, h, c_2\}$	$\{o, h, c_1, c_2\}$	1
	$\{o, h, c_1, c_2\}$	$\{o, h, c_1\}$ or $\{o, h, c_1, c_2\}$	2
$\{o, h, c_1, c_2\}$	$\{o, h, c_1\}$	$\{o, h, c_1\}$ or $\{o, h, c_1, c_2\}$	2
	$\{o, h, c_2\}$	$\{o, h, c_2\}$ or $\{o, h, c_1, c_2\}$	2

Table S7: The finally remaining possible combinations of γ-β restrictions for $ohc_1^*c_2$-variants with $\Gamma_2^{120^\circ} = \{o, h, c_2\}$

$\Gamma_2^{80^\circ}$	$\Gamma_3^{80^\circ}$	$\Gamma_3^{120^\circ}$	Count
$\{o, h, c_1, c_2\}$	$\{o, h, c_1\}$	$\{o, h, c_1\}$ or $\{o, h, c_1, c_2\}$	2
	$\{o, h, c_2\}$	$\{o, h, c_1, c_2\}$	1

complex than those including less states, which may seem counterintuitive. However, this is because the variants including less Markov states assume stronger and/or more delicate interactions between the γ- and β-subunits (in the form of γ-β restrictions), which could result in bias and over-selection of the states.

Table S8: The finally remaining 5 $ohc_1^*c_2^*$-variants and 10 $ohc_1^*c_2$-variants, classified into five groups

Group	Number of Markov states	Number of $ohc_1^*c_2^*$-variants	Number of $ohc_1^*c_2$-variants
1	972	0	2
2	891	0	1
3	864	2	3
4	810	2	3
5	702	1	1

To find the minimal ohc_1c_2-variant that explains all available experimental data, we naturally started searching from the simplest variants. To decide whether the second closed conformation c_2 is also catalytically active, the selection covered both $ohc_1^*c_2^*$- and $ohc_1^*c_2$-variants (γ-β restrictions shown in Table 3, second column). We first selected the two simplest $ohc_1^*c_2^*$-variants (from group 3, termed $ohc_1^*c_2^*$-$m.1$ and $ohc_1^*c_2^*$-$m.2$) for detailed investigation following the previously introduced training-validation procedure (Subsection 2.2). For direct comparison, we also investigated the two $ohc_1^*c_2$-variants from group 3 with

identical γ-β restrictions. Additionally, we investigated one of the two simplest $ohc_1^*c_2$-variants (from group 1, termed $ohc_1^*c_2$-w). The performance of these two $ohc_1^*c_2^*$- and three $ohc_1^*c_2$-variants are reported in the main article (Subsection 2.4).

Notably, we consider these five selected ohc_1c_2-variants the most plausible ones. We did not extensively investigate the other ten ohc_1c_2-variants, but a brief analysis shows that they are either subsets of the selected ohc_1c_2-variants and therefore do not require extra testing, or less plausible and likely to disagree with some experimental data:

(1) The two ohc_1c_2-variants in group 5 (including one $ohc_1^*c_2^*$-variant and one $ohc_1^*c_2$-variant) with identical γ-β restrictions (Supplementary Tables S9) are actually subsets of variants ohc_1c_2-m.1 or variants ohc_1c_2-m.2.

(2) The two $ohc_1^*c_2^*$-variants in group 4 and those two $ohc_1^*c_2$-variants with identical $\{\Gamma_{1,2,3}^{80°,120°}\}$ (Supplementary Table S10) are unlikely to reproduce the observed population shift from the 120°-states to the 80°-states with increasing ATP concentration. With both $\{\Gamma_{1,2,3}^{80°,120°}\}$ shown in Supplementary Table S10, at 120°, all the three β-subunits are restricted from the most stable conformation (c_2 for the first set, c_1 for the second set). Therefore, it is likely that the 120°-states are of higher free energies than the 80°-states even at substantially low ATP concentration.

(3) The other four $ohc_1^*c_2$-variants from groups 1–4 respectively (Supplementary Table S11) are unlikely to reproduce the measured binding affinities of F_1-ATPase locked within the 80°-dwell [22]. In these four $ohc_1^*c_2$-variants, because only c_1 is catalytically active, the microscopic ATP binding affinity of c_1 should be higher than that of c_2. According to the analysis in Supplementary Section S5, the apparent binding affinities of β_2 and β_3 in F_1-ATPase locked within the 80°-dwell are limited by the microscopic binding affinity of c_1, and therefore of similar magnitudes, contradicting the measurements showing three distinct binding affinities [22].

Table S9: γ-β restrictions of the two ohc_1c_2-variants in group 5

ϕ	β_1	β_2	β_3
80°	o, h	o, h, c_1	o, h, c_2
120°	o	o, h	o, h, c_1, c_2

Table S10: γ-β restrictions of the four ohc_1c_2-variants in group 4

ϕ	β_1	β_2	β_3
80°	o, h	o, h, c_1	o, h, c_1, c_2
120°	o	o, h	o, h, c_1

ϕ	β_1	β_2	β_3
80°	o, h	o, h, c_1, c_2	o, h, c_2
120°	o	o, h	o, h, c_2

Table S11: γ-β restrictions of the other four $ohc_1^*c_2$-variants from group 1–4 respectively

ϕ	β_1	β_2	β_3
80°	o, h	o, h, c_1, c_2	o, h, c_1
120°	o	o, h, c_2	o, h, c_1, c_2

ϕ	β_1	β_2	β_3
80°	o, h	o, h, c_1, c_2	o, h, c_1
120°	o	o, h, c_2	o, h, c_1

ϕ	β_1	β_2	β_3
80°	o, h	o, h, c_1, c_2	o, h, c_1
120°	o	o, h	o, h, c_1, c_2

ϕ	β_1	β_2	β_3
80°	o, h	o, h, c_1, c_2	o, h, c_1
120°	o	o, h	o, h, c_1

S5 Analytical expressions of the ADP binding affinities in terms of the model parameters

Here, we derive analytical expressions for the apparent ADP binding affinities (Methods) in terms of the parameters of our Markov model, particularly the free energies. The apparent binding affinities $\{K_k\}$ are obtained by fitting an ADP titration curve to the equilibrium binding model [20–22]:

$$\nu(c_{\mathrm{D}}) = \sum_{k=1}^{3} \frac{c_{\mathrm{D}}}{c_{\mathrm{D}} + K_k}, \tag{S5.1}$$

where ν is the total occupancy of the binding sites; c_{D} is the concentration of ADP; the summation is over all the three binding sites within F_1-ATPase. Our aim is to derive an expression for ν in terms of the free energies as well as ADP concentration c_{D} which will then be compared to Equation (S5.1) to obtain the expressions of $\{K_k\}$.

Within our Markov model, the total occupancy ν is evaluated by the ensemble average of the numbers of occupied catalytic sites $\{n_i\}$ of the Markov states $\{i\}$ in the steady-state of the system where the populations of the states are $\{\rho_i^{\mathrm{st}}\}$ (Equation (11)). To obtain the steady-state populations analytically, we use the Boltzmann distribution approximation. For ADP titration, ADP concentration is varied in a large range, whereas ATP concentration is typically low. Under this condition, the net rate of ATP hydrolysis/synthesis is typically small, and the populations of the Markov states with ATP-bound β-subunits (which result from reversible ATP synthesis in the catalytically active sites) are also low and can be ignored. Therefore, the steady-state distribution is expected to approach the Boltzmann distribution of those Markov states including only empty and ADP-bound β-subunits, where ADP binding and release within each β-subunit is in equilibrium.

In the Boltzmann distribution, the population of a state i including only empty and/or ADP-bound β-subunits depends on its free energy G_i:

$$\rho_i = \frac{1}{Z} \exp(-G_i/k_{\mathrm{B}}T), \tag{S5.2}$$

where T is the temperature and Z is the partition function for normalizing the distribution,

$$Z = \sum_i \exp(-G_i/k_{\mathrm{B}}T), \tag{S5.3}$$

where the summation is over all these states. Due to the three-fold pseudo-symmetry of F_1-ATPase, we only need to consider those states where the γ-subunit is at 80° or 120°.

For these states, the free energies are (adapted from Equations (2)-(4))

$$G(\mathbf{s}, c_{\mathrm{D}}) = \sum_{k=1,2,3} G_{\beta,\mathcal{C}^{(k)}} + \sum_{\{k|\mathcal{B}^{(k)}=\mathrm{D}\}} \left(\Delta G^{\ominus}_{\mathrm{b},\mathcal{C}^{(k)},\mathrm{D}} - k_{\mathrm{B}}T \ln c_{\mathrm{D}}\right) + G_{\gamma\beta}(\phi), \quad \text{(S5.4)}$$

where $G_{\gamma\beta} = -2.3\, k_{\mathrm{B}}T$ if and only if the γ-subunit is at 120° ($\phi = 120°$; at this orientation, β_1 can only adopt the o conformation); otherwise, $G_{\gamma\beta} = 0$. The second term in Equation (S5.4) includes summation only over the ADP-bound β-subunit(s). The contribution to the partition function by this state is

$$\begin{aligned} Z(\mathbf{s}, c_{\mathrm{D}}) &= \exp\left(-\frac{G(\mathbf{s}, c_{\mathrm{D}})}{k_{\mathrm{B}}T}\right) \\ &= \exp\left(-\frac{G^{\ominus}(\mathbf{s})}{k_{\mathrm{B}}T}\right) c_{\mathrm{D}}^{b_1+b_2+b_3} \\ &\equiv Z^{\ominus}(\mathbf{s}) c_{\mathrm{D}}^{b_1+b_2+b_3}. \end{aligned} \quad \text{(S5.5)}$$

Here, $b_k = 0$ and 1 ($k = 1, 2, 3$) for empty and ADP-bound β_k respectively; $G^{\ominus}(\mathbf{s})$ is the [ADP]-independent part $G^{\ominus}(\mathbf{s})$ of the free energy of the state $\mathbf{s}$:

$$G^{\ominus}(\mathbf{s}) = \sum_{k=1,2,3} G_{\beta,\mathcal{C}^{(k)}} + \sum_{\{k|\mathcal{B}^{(k)}=\mathrm{D}\}} \Delta G^{\ominus}_{\mathrm{b},\mathcal{C}^{(k)},\mathrm{D}} + G_{\gamma\beta}(\phi), \quad \text{(S5.6)}$$

and $Z^{\ominus}(\mathbf{s})$ is defined

$$Z^{\ominus}(\mathbf{s}) = \exp(-G^{\ominus}(\mathbf{s})/k_{\mathrm{B}}T). \quad \text{(S5.7)}$$

The total occupancy ν is (adapted from Equation (11))

$$\nu(c_{\mathrm{D}}) = \sum_{\mathbf{s}} b(\mathbf{s})\rho(\mathbf{s}), \quad \text{(S5.8)}$$

where $b(\mathbf{s}) = (b_1 + b_2 + b_3)$ is the number of occupied binding sites in state $\mathbf{s}$. Accordingly, ν is expressed in terms of $Z^{\ominus}(\mathbf{s})$ by:

$$\begin{aligned} \nu(c_{\mathrm{D}}) &= \frac{\sum_{\mathbf{s}} b(\mathbf{s}) Z^{\ominus}(\mathbf{s}) c_{\mathrm{D}}^{b(\mathbf{s})}}{\sum_{\mathbf{s}} Z^{\ominus}(\mathbf{s}) c_{\mathrm{D}}^{b(\mathbf{s})}} \\ &= \frac{\sum\limits_{b(\mathbf{s})=1} Z^{\ominus}(\mathbf{s}) c_{\mathrm{D}} + 2\sum\limits_{b(\mathbf{s})=2} Z^{\ominus}(\mathbf{s}) c_{\mathrm{D}}^2 + 3\sum\limits_{b(\mathbf{s})=3} Z^{\ominus}(\mathbf{s}) c_{\mathrm{D}}^3}{\sum\limits_{b(\mathbf{s})=0} Z^{\ominus}(\mathbf{s}) + \sum\limits_{b(\mathbf{s})=1} Z^{\ominus}(\mathbf{s}) c_{\mathrm{D}} + \sum\limits_{b(\mathbf{s})=2} Z^{\ominus}(\mathbf{s}) c_{\mathrm{D}}^2 + \sum\limits_{b(\mathbf{s})=3} Z^{\ominus}(\mathbf{s}) c_{\mathrm{D}}^3} \\ &\equiv \frac{W_1 c_{\mathrm{D}} + 2W_2 c_{\mathrm{D}}^2 + 3W_3 c_{\mathrm{D}}^3}{W_0 + W_1 c_{\mathrm{D}} + W_2 c_{\mathrm{D}}^2 + W_3 c_{\mathrm{D}}^3}, \end{aligned} \quad \text{(S5.9)}$$

with

$$
\begin{aligned}
W_0 &= \sum_{b(\mathbf{s})=0} Z^{\Theta}(\mathbf{s}) = \sum_{b_{1,2,3}=0} Z^{\Theta}(\mathbf{s}), \\
W_1 &= \sum_{b(\mathbf{s})=1} Z^{\Theta}(\mathbf{s}), \\
W_2 &= \sum_{b(\mathbf{s})=2} Z^{\Theta}(\mathbf{s}), \\
W_3 &= \sum_{b(\mathbf{s})=3} Z^{\Theta}(\mathbf{s}) = \sum_{b_{1,2,3}=1} Z^{\Theta}(\mathbf{s}).
\end{aligned} \tag{S5.10}
$$

Here, " $\sum_{b(\mathbf{s})=m}$ " $(m = 0, 1, 2, 3)$ represents the summation over all the states $\mathbf{s}$ where $b(\mathbf{s}) = m$.

Equation (S5.1) for $N = 3$ can be written as

$$
\nu(c_{\mathrm{D}}) = \frac{\left(\sum_{j<k} K_j K_k\right) c_{\mathrm{D}} + 2\left(\sum_{k} K_k\right) c_{\mathrm{D}}^2 + 3c_{\mathrm{D}}^3}{K_1K_2K_3 + \left(\sum_{j<k} K_j K_k\right) c_{\mathrm{D}} + \left(\sum_{k} K_k\right) c_{\mathrm{D}}^2 + c_{\mathrm{D}}^3}, \tag{S5.11}
$$

with $j, k = 1, 2, 3$. Comparing Equation (S5.9) to Equation (S5.11), it is found that

$$
\begin{aligned}
K_1K_2K_3 &= W_0/W_3, \\
K_1K_2 + K_1K_3 + K_2K_3 &= W_1/W_3, \\
K_1 + K_2 + K_3 &= W_2/W_3,
\end{aligned} \tag{S5.12}
$$

which implies that the apparent binding affinities K_1, K_2 and K_3 are the three roots of the cubic equation

$$
W_3x^3 - W_2x^2 + W_1x - W_0 = 0. \tag{S5.13}
$$

Notably, the physical meaning of the binding affinities require K_1, K_2 and K_3 to be positive real numbers, whereas there is no guarantee (at least not clear yet) that Equation (S5.13) has three real roots. If Equation (S5.13) does have three real roots, these three roots must be positive considering Equation (S5.10) which shows $W_{0,1,2,3} > 0$ and Equation (S5.12). In this case, Equation (S5.12) provides a general analytical solution for the apparent binding affinities obtained by fitting the ADP titration curve predicted by our model to Equation (S5.1).

However, if Equation (S5.13) does not have three real roots, it must have one real positive root and two conjugate complex roots. In this case, the apparent binding affinities obtained by fitting the predicted ADP titration curve to Equation (S5.1) are likely different from those given by Equation (S5.12).

While Equation (S5.12) is general, it is rather complicated and unstraightforward. Below, we attempt to derive a more specific but simpler and easier-to-interpret expression for the apparent binding affinities.

Plug Equations (S5.7) and (S5.6) into Equation (S5.10), we obtain

$$
\begin{aligned}
W_0 &= \sum_{(\phi,\mathcal{C}^{(1)},\mathcal{C}^{(2)},\mathcal{C}^{(3)})} Z^{\mathrm{conf}}, \\
W_1 &= \sum_{(\phi,\mathcal{C}^{(1)},\mathcal{C}^{(2)},\mathcal{C}^{(3)})} Z^{\mathrm{conf}} \sum_{k=1,2,3} \exp\left(-\frac{\Delta G^{\Theta}_{\mathrm{b},\mathcal{C}^{(k)},\mathrm{D}}}{k_{\mathrm{B}}T}\right), \\
W_2 &= \sum_{(\phi,\mathcal{C}^{(1)},\mathcal{C}^{(2)},\mathcal{C}^{(3)})} Z^{\mathrm{conf}} \sum_{j<k} \exp\left(-\frac{\Delta G^{\Theta}_{\mathrm{b},\mathcal{C}^{(j)},\mathrm{D}}}{k_{\mathrm{B}}T}\right) \exp\left(-\frac{\Delta G^{\Theta}_{\mathrm{b},\mathcal{C}^{(k)},\mathrm{D}}}{k_{\mathrm{B}}T}\right), \\
W_3 &= \sum_{(\phi,\mathcal{C}^{(1)},\mathcal{C}^{(2)},\mathcal{C}^{(3)})} Z^{\mathrm{conf}} \prod_{k=1,2,3} \exp\left(-\frac{\Delta G^{\Theta}_{\mathrm{b},\mathcal{C}^{(k)},\mathrm{D}}}{k_{\mathrm{B}}T}\right),
\end{aligned}
\tag{S5.14}
$$

where the summation "$\sum_{(\phi,\mathcal{C}^{(1)},\mathcal{C}^{(2)},\mathcal{C}^{(3)})}$" is over all the possible combinations of γ-orientations ($\phi = 80°$, $120°$) and β-subunit conformations ($\mathcal{C}^{(k)} \in \Gamma_k^{\phi}$, $k = 1, 2, 3$); Z^{conf} is defined

$$
Z^{\mathrm{conf}}(\phi, \mathcal{C}^{(1)}, \mathcal{C}^{(2)}, \mathcal{C}^{(3)}) = \exp\left(-\frac{G_{\gamma\beta}(\phi)}{k_{\mathrm{B}}T}\right) \prod_{k=1,2,3} \exp\left(-\frac{G_{\beta,\mathcal{C}^{(k)}}}{k_{\mathrm{B}}T}\right). \tag{S5.15}
$$

For simplicity of the equations to be presented further, we define the following equilibrium constants

$$
\begin{aligned}
K_{\mathrm{I},\phi} &= \exp\left(-\frac{G_{\gamma\beta}(\phi)}{k_{\mathrm{B}}T}\right), \\
K_{\beta,\mathcal{C}} &= \exp\left(-\frac{G_{\beta,\mathcal{C}}}{k_{\mathrm{B}}T}\right), \\
K_{\mathrm{b},\mathcal{C}} &= \exp\left(-\frac{\Delta G^{\Theta}_{\mathrm{b},\mathcal{C}}}{k_{\mathrm{B}}T}\right),
\end{aligned}
\tag{S5.16}
$$

for $\mathcal{C}$ being all the β-subunit conformations included in the variant, *i.e.*, $\mathcal{C} = o, h, c$ for *ohc*-variants, and $\mathcal{C} = o, h, c_1, c_2$ for *ohc*$_1$*c*$_2$-variants.

F_1-ATPase locked in 80°- or 120°-dwell We first consider a simpler case where F_1-ATPase is locked in the catalytic dwell at 80°, *e.g.*, by disulfide crosslinking [22]. In this case, ϕ can only be 80°, while each of the three β-subunits could freely and independently choose any conformation $\mathcal{C}^{(k)} \in \Gamma_k^{80°}$, and the summation $\sum_{(\phi,\mathcal{C}^{(1)},\mathcal{C}^{(2)},\mathcal{C}^{(3)})}$ can be dissected into the triple sum $\sum_{\mathcal{C}^{(1)}}\sum_{\mathcal{C}^{(2)}}\sum_{\mathcal{C}^{(3)}}$ omitting ϕ. Additionally, $K_{\mathrm{I},\phi} = 1$. Accordingly, and using the definitions in Equation (S5.16), W_0 and W_1 in Equation (S5.14) are converted to

$$\begin{aligned} W_0 &= \prod_{k=1,2,3}\left(\sum_{\mathcal{C}^{(k)}} K_{\beta,\mathcal{C}^{(k)}}\right), \\ W_1 &= \sum_{(i,j,k)}\left[\left(\sum_{\mathcal{C}^{(i)}} K_{\beta,\mathcal{C}^{(i)}}K_{\mathrm{b},\mathcal{C}^{(i)}}\right)\left(\sum_{\mathcal{C}^{(j)}} K_{\beta,\mathcal{C}^{(j)}}\right)\left(\sum_{\mathcal{C}^{(k)}} K_{\beta,\mathcal{C}^{(k)}}\right)\right], \end{aligned} \tag{S5.17}$$

where the summation $\sum_{(i,j,k)}$ is over $(i,j,k) \in \{(1,2,3),(2,1,3),(3,1,2)\}$. Accordingly,

$$\frac{W_1}{W_0} = \frac{\sum_{\mathcal{C}^{(1)}} K_{\beta,\mathcal{C}^{(1)}}K_{\mathrm{b},\mathcal{C}^{(1)}}}{\sum_{\mathcal{C}^{(1)}} K_{\beta,\mathcal{C}^{(1)}}} + \frac{\sum_{\mathcal{C}^{(2)}} K_{\beta,\mathcal{C}^{(2)}}K_{\mathrm{b},\mathcal{C}^{(2)}}}{\sum_{\mathcal{C}^{(2)}} K_{\beta,\mathcal{C}^{(2)}}} + \frac{\sum_{\mathcal{C}^{(3)}} K_{\beta,\mathcal{C}^{(3)}}K_{\mathrm{b},\mathcal{C}^{(3)}}}{\sum_{\mathcal{C}^{(3)}} K_{\beta,\mathcal{C}^{(3)}}}. \tag{S5.18}$$

Comparing this Equation (S5.18) to $W_1/W_0 = 1/K_1 + 1/K_2 + 1/K_3$ (given by Equation (S5.12)), each term in Equation (S5.18) is attributed to the apparent binding affinity of one β-subunit,

$$\frac{1}{K_k} = \frac{\sum_{\mathcal{C}\in\Gamma_k^{80°}} K_{\beta,\mathcal{C}}K_{\mathrm{b},\mathcal{C}}}{\sum_{\mathcal{C}\in\Gamma_k^{80°}} K_{\beta,\mathcal{C}}}. \tag{S5.19}$$

It is easy to verify that K_k given in Equation (S5.19) satisfy Equation (S5.12).

Equation (S5.19) can be written in a more symmetric form

$$(K_k^{80°})^{-1} = \frac{1}{\sum_{\mathcal{C}\in\Gamma_k^{80°}} K_{\beta,\mathcal{C}}} \sum_{\mathcal{C}\in\Gamma_k^{80°}} K_{\beta,\mathcal{C}}(K_{\mathrm{d},\mathcal{C}})^{-1}, \tag{S5.20}$$

where $K_{\mathrm{d},\mathcal{C}} = \exp(G_{\mathrm{b},\mathcal{C}}/k_{\mathrm{B}}T)$. Here, we use the superscript 80° in the apparent binding affinity $K_k^{80°}$ to emphasize that this equation is derived for F_1-ATPase stalled at 80°.

In contrast to $K_{1,2,3}$ which are interpreted as the *apparent* binding affinities (dissociation constants) of the β-subunits, $K_{\mathrm{d},\mathcal{C}}$ including $K_{\mathrm{d},o}$, $K_{\mathrm{d},h}$ and $K_{\mathrm{d},c}$ (in *ohc*-variants) or $K_{\mathrm{d},o}$, $K_{\mathrm{d},h}$, K_{d,c_1} and K_{d,c_2} (in ohc_1c_2-variants) can be interpreted as the *microscopic* binding affinities (dissociation constants) of the β-subunit conformations included in our Markov model. According to this Equation (S5.20), the *apparent* binding affinity of a β-subunit is a superposition (weighted average) of the *microscopic* binding affinities of the several conformations this β-subunit can adopt, with weights $K_{\beta,\mathcal{C}}$ as the Boltzmann factors of the conformational energies $G_{\beta,\mathcal{C}}$ (Equation (S5.16)).

For F_1-ATPase locked in the ATP-waiting dwell ($\phi = 120°$ exclusively), similar derivation can be done, which leads to

$$(K_k^{120°})^{-1} = \frac{1}{\sum\limits_{\mathcal{C}\in\Gamma_k^{120°}} K_{\beta,\mathcal{C}}} \sum_{\mathcal{C}\in\Gamma_k^{120°}} K_{\beta,\mathcal{C}}(K_{\mathrm{d},\mathcal{C}})^{-1}, \tag{S5.21}$$

of exactly the same form with Equation (S5.20) derived for F_1-ATPase stalled at 80°. The additional favorable interaction energy between the γ- and β_1-subunit is cancelled-out and therefore does not appear in Equation (S5.21). Notably, because we assumed $\Gamma_1^{120°} = \{o\}$, the apparent binding affinity of β_1 in F_1-ATPase stalled at 120° is simply the microscopic binding affinity of the *o* conformation.

Equations (S5.20) and (S5.21) can be summarized into one equation:

$$(K_k^{\phi})^{-1} = \frac{1}{\Omega_k} \sum_{\mathcal{C}\in\Gamma_k^{\phi}} K_{\beta,\mathcal{C}}(K_{\mathrm{d},\mathcal{C}})^{-1}, \text{with}\, \Omega_k = \sum_{\mathcal{C}\in\Gamma_k^{\phi}} K_{\beta,\mathcal{C}}. \tag{S5.22}$$

This equation can be generalized to freely-rotating F_1-ATPase by defining the concept of apparent binding affinity K_k^{ϕ} of the β_k-subunit at a particular γ-orientation ϕ, which provides a simplified representation of the set of accessible conformations of the β_k-subunit at ϕ (*i.e.*, Γ_k^{ϕ}), and, can be considered as a measure for the "open-ness" of β_k.

An important conclusion from Equation (S5.22) is that if two β-subunits are allowed to adopt the same set of conformations at a γ-orientation ϕ (*i.e.*, $\Gamma_k^{\phi} = \Gamma_j^{\phi}$), their apparent binding affinities at this γ-orientation are likely very similar. The ADP titration curves measured on F_1-ATPase locked into the catalytic and ATP-waiting dwells suggest three distinct binding affinities within both dwells [22]. Therefore, we excluded those ohc_1c_2-variants assuming identical

γ-β restrictions Γ_k^{ϕ} for two β-subunits at the same γ-orientation (Supplementary Section S4).

Freely-rotating F_1-ATPase For freely-rotating F_1-ATPase, the summations over ϕ in W_0 and W_1 (Equation (S5.14)) must be preserved, due to which the factorization of the three β-subunits like in Equation (S5.17) is not always possible. However, if the γ-β restrictions for a β-subunit are identical at 80° and 120° (*e.g.*, for β_k, $\Gamma_k^{80^\circ} = \Gamma_k^{120^\circ}$), the summations over the conformations of this β-subunit in W_0 and W_1 can be factorized out:

$$W_0 = \left(\sum_{\mathcal{C}^{(k)}} K_{\beta,\mathcal{C}^{(k)}}\right)\left(\sum_{(\phi,\mathcal{C}^{(i)},\mathcal{C}^{(j)})} K_{\mathrm{I},\phi} K_{\beta,\mathcal{C}^{(i)}} K_{\beta,\mathcal{C}^{(j)}}\right), \tag{S5.23}$$

$$\begin{aligned} W_1 = &\left(\sum_{\mathcal{C}^{(k)}} K_{\beta,\mathcal{C}^{(k)}} K_{\mathrm{b},\mathcal{C}^{(k)}}\right)\left(\sum_{(\phi,\mathcal{C}^{(i)},\mathcal{C}^{(j)})} K_{\mathrm{I},\phi} K_{\beta,\mathcal{C}^{(i)}} K_{\beta,\mathcal{C}^{(j)}}\right) \\ &+ \left(\sum_{\mathcal{C}^{(k)}} K_{\beta,\mathcal{C}^{(k)}}\right)\left(\sum_{(\phi,\mathcal{C}^{(i)},\mathcal{C}^{(j)})} K_{\mathrm{I},\phi} K_{\beta,\mathcal{C}^{(i)}} K_{\beta,\mathcal{C}^{(j)}} (K_{\mathrm{b},\mathcal{C}^{(i)}} + K_{\mathrm{b},\mathcal{C}^{(j)}})\right), \end{aligned} \tag{S5.24}$$

thus the ratio is

$$\frac{W_1}{W_0} = \frac{\sum_{\mathcal{C}^{(k)}} K_{\beta,\mathcal{C}^{(k)}} K_{\mathrm{b},\mathcal{C}^{(k)}}}{\sum_{\mathcal{C}^{(k)}} K_{\beta,\mathcal{C}^{(k)}}} + \frac{\sum_{(\phi,\mathcal{C}^{(i)},\mathcal{C}^{(j)})} K_{\mathrm{I},\phi} K_{\beta,\mathcal{C}^{(i)}} K_{\beta,\mathcal{C}^{(j)}} (K_{\mathrm{b},\mathcal{C}^{(i)}} + K_{\mathrm{b},\mathcal{C}^{(j)}})}{\sum_{(\phi,\mathcal{C}^{(i)},\mathcal{C}^{(j)})} K_{\mathrm{I},\phi} K_{\beta,\mathcal{C}^{(i)}} K_{\beta,\mathcal{C}^{(j)}}}, \tag{S5.25}$$

and we attribute the first term in Equation (S5.25) to K_k:

$$(K_k)^{-1} = \frac{1}{\Omega_k} \sum_{\mathcal{C}\in\Gamma_k^{\phi}} K_{\beta,\mathcal{C}} (K_{\mathrm{d},\mathcal{C}})^{-1}, \text{with } \Omega_k = \sum_{\mathcal{C}\in\Gamma_k^{\phi}} K_{\beta,\mathcal{C}}, \tag{S5.26}$$

where $\Gamma_k^{\phi} = \Gamma_k^{80^\circ} = \Gamma_k^{120^\circ}$. We say that this β_k-subunit is "decoupled" whereas the other two β-subunit are "coupled" due to the indirect interaction mediated via the γ-subunit,

$$\begin{aligned} (K_i)^{-1} + (K_j)^{-1} &= \frac{1}{\Omega_{(i,j)}} \sum_{(\phi,\mathcal{C}^{(i)},\mathcal{C}^{(j)})} \omega_{\phi,\mathcal{C}^{(i)},\mathcal{C}^{(j)}} \left((K_{\mathrm{d},\mathcal{C}^{(i)}})^{-1} + (K_{\mathrm{d},\mathcal{C}^{(j)}})^{-1}\right), \\ (K_i)^{-1}(K_j)^{-1} &= \frac{1}{\Omega_{(i,j)}} \sum_{(\phi,\mathcal{C}^{(i)},\mathcal{C}^{(j)})} \omega_{\phi,\mathcal{C}^{(i)},\mathcal{C}^{(j)}} (K_{\mathrm{d},\mathcal{C}^{(i)}})^{-1} (K_{\mathrm{d},\mathcal{C}^{(j)}})^{-1}, \\ \text{with} \quad \omega_{\phi,\mathcal{C}^{(i)},\mathcal{C}^{(j)}} &= K_{\mathrm{I},\phi} K_{\beta,\mathcal{C}^{(i)}} K_{\beta,\mathcal{C}^{(j)}}, \quad \Omega_{(i,j)} = \sum_{(\phi,\mathcal{C}^{(i)},\mathcal{C}^{(j)})} \omega_{\phi,\mathcal{C}^{(i)},\mathcal{C}^{(j)}}. \end{aligned} \tag{S5.27}$$

If the γ-β restrictions for another β-subunit are also identical at 80° and 120° (*e.g.*, for β_j, $\Gamma_j^{80^\circ} = \Gamma_j^{120^\circ}$), the summations over the conformations of this β-subunit in W_0 and W_1 can be further factorized out, *i.e.*, Equations (S5.23) and (S5.24) can be further converted to

$$W_0 = \left(\sum_{\mathcal{C}^{(k)}} K_{\beta,\mathcal{C}^{(k)}}\right)\left(\sum_{\mathcal{C}^{(j)}} K_{\beta,\mathcal{C}^{(j)}}\right)\left(\sum_{(\phi,\mathcal{C}^{(i)})} K_{\mathrm{I},\phi} K_{\beta,\mathcal{C}^{(i)}}\right), \tag{S5.28}$$

$$\begin{aligned} W_1 = &\left(\sum_{\mathcal{C}^{(k)}} K_{\beta,\mathcal{C}^{(k)}} K_{\mathrm{b},\mathcal{C}^{(k)}}\right)\left(\sum_{\mathcal{C}^{(j)}} K_{\beta,\mathcal{C}^{(j)}}\right)\left(\sum_{(\phi,\mathcal{C}^{(i)})} K_{\mathrm{I},\phi} K_{\beta,\mathcal{C}^{(i)}}\right) \\ &+ \left(\sum_{\mathcal{C}^{(k)}} K_{\beta,\mathcal{C}^{(k)}}\right)\left(\sum_{\mathcal{C}^{(j)}} K_{\beta,\mathcal{C}^{(j)}} K_{\mathrm{b},\mathcal{C}^{(j)}}\right)\left(\sum_{(\phi,\mathcal{C}^{(i)})} K_{\mathrm{I},\phi} K_{\beta,\mathcal{C}^{(i)}}\right) \\ &+ \left(\sum_{\mathcal{C}^{(k)}} K_{\beta,\mathcal{C}^{(k)}}\right)\left(\sum_{\mathcal{C}^{(j)}} K_{\beta,\mathcal{C}^{(j)}}\right)\left(\sum_{(\phi,\mathcal{C}^{(i)})} K_{\mathrm{I},\phi} K_{\beta,\mathcal{C}^{(i)}} K_{\mathrm{b},\mathcal{C}^{(i)}}\right), \end{aligned} \tag{S5.29}$$

thus the ratio is

$$\frac{W_1}{W_0} = \frac{\sum_{\mathcal{C}^{(k)}} K_{\beta,\mathcal{C}^{(k)}} K_{\mathrm{b},\mathcal{C}^{(k)}}}{\sum_{\mathcal{C}^{(k)}} K_{\beta,\mathcal{C}^{(k)}}} + \frac{\sum_{\mathcal{C}^{(j)}} K_{\beta,\mathcal{C}^{(j)}} K_{\mathrm{b},\mathcal{C}^{(j)}}}{\sum_{\mathcal{C}^{(j)}} K_{\beta,\mathcal{C}^{(j)}}} + \frac{\sum_{(\phi,\mathcal{C}^{(i)})} K_{\mathrm{I},\phi} K_{\beta,\mathcal{C}^{(i)}} K_{\mathrm{b},\mathcal{C}^{(i)}}}{\sum_{(\phi,\mathcal{C}^{(i)})} K_{\mathrm{I},\phi} K_{\beta,\mathcal{C}^{(i)}}}, \tag{S5.30}$$

and we attribute the three terms in Equation (S5.30) to K_k, K_j and K_i respectively:

$$(K_i)^{-1} = \frac{1}{\Omega_i} \sum_{(\phi,\mathcal{C}^{(i)})} K_{\mathrm{I},\phi} K_{\beta,\mathcal{C}^{(i)}} (K_{\mathrm{d},\mathcal{C}^{(i)}})^{-1}, \text{with}\, \Omega_i = \sum_{(\phi,\mathcal{C}^{(i)})} K_{\mathrm{I},\phi} K_{\beta,\mathcal{C}^{(i)}}, \tag{S5.31}$$

$$(K_j)^{-1} = \frac{1}{\Omega_j} \sum_{\mathcal{C}\in\Gamma_j^{\phi}} K_{\beta,\mathcal{C}} (K_{\mathrm{d},\mathcal{C}})^{-1}, \text{with}\, \Omega_j = \sum_{\mathcal{C}\in\Gamma_j^{\phi}} K_{\beta,\mathcal{C}},$$

$$(K_k)^{-1} = \frac{1}{\Omega_k} \sum_{\mathcal{C}\in\Gamma_k^{\phi}} K_{\beta,\mathcal{C}} (K_{\mathrm{d},\mathcal{C}})^{-1}, \text{with}\, \Omega_k = \sum_{\mathcal{C}\in\Gamma_k^{\phi}} K_{\beta,\mathcal{C}}. \tag{S5.32}$$

where $\Gamma_j^{\phi} = \Gamma_j^{80^\circ} = \Gamma_j^{120^\circ}$ and $\Gamma_k^{\phi} = \Gamma_k^{80^\circ} = \Gamma_k^{120^\circ}$. Here, all the three β-subunits are "decoupled".

More explicitly, Equation (S5.31) is

$$(K_i)^{-1} = \frac{1}{\Omega_i}\left(\sum_{\mathcal{C}\in\Gamma_i^{80^\circ}} K_{\beta,\mathcal{C}} (K_{\mathrm{d},\mathcal{C}})^{-1} + K_{\mathrm{I}} \sum_{\mathcal{C}\in\Gamma_i^{120^\circ}} K_{\beta,\mathcal{C}} (K_{\mathrm{d},\mathcal{C}})^{-1}\right), \tag{S5.33}$$

where $K_{\mathrm{I}} \equiv K_{\mathrm{I},120^\circ} = 10$, and

$$\Omega_i = \sum_{\mathcal{C}\in\Gamma_i^{80^\circ}} K_{\beta,\mathcal{C}} + K_{\mathrm{I}} \sum_{\mathcal{C}\in\Gamma_i^{120^\circ}} K_{\beta,\mathcal{C}}. \tag{S5.34}$$

Notably, the additional favorable interaction energy between the γ- and β_1-subunits takes effect in the apparent binding affinity of β_i, the only β-subunit whose $\Gamma_i^{80^\circ} \neq \Gamma_i^{120^\circ}$, as an extra weight K_{I} on the 120°-conformations, even though β_i may or may not be β_1.

Application to particular variants These analytical expressions of the apparent ADP binding affinities in terms of the model parameters explain why variant *ohc*-s* reproduces the measured ADP binding affinities [21] whereas variant *ohc*-w* does not (Results and Discussion).

For both variants *ohc*-s* and *ohc*-w*, the three β-subunits are *decoupled*. For variant *ohc*-w*, applying Equations (S5.32) and (S5.33),

$$\begin{aligned}(K_1)^{-1} =& \frac{1}{\Omega_1}\left((1+K_{\mathrm{I}})K_{\beta,o}(K_{\mathrm{d},o})^{-1} + K_{\beta,h}(K_{\mathrm{d},h})^{-1}\right),\\ \text{with}\quad \Omega_1 =& (1+K_{\mathrm{I}})K_{\beta,o} + K_{\beta,h};\end{aligned} \tag{S5.35}$$

$$\begin{aligned}(K_2)^{-1} = (K_3)^{-1} =& \frac{1}{\Omega_{2,3}}\left(K_{\beta,o}(K_{\mathrm{d},o})^{-1} + K_{\beta,h}(K_{\mathrm{d},h})^{-1} + K_{\beta,c}(K_{\mathrm{d},c})^{-1}\right),\\ \text{with}\quad \Omega_{2,3} =& K_{\beta,o} + K_{\beta,h} + K_{\beta,c}.\end{aligned} \tag{S5.36}$$

Equation (S5.36) suggests that the apparent binding affinities of β_2 and β_3 are likely very close, which has been corroborated by the numerical results (Supplementary Figure S1).

In contrast, for variant *ohc*-s*,

$$\begin{aligned}(K_1)^{-1} =& (K_{\mathrm{d},o})^{-1};\\ (K_2)^{-1} =& \frac{1}{\Omega_2}\left((1+K_{\mathrm{I}})K_{\beta,o}(K_{\mathrm{d},o})^{-1} + K_{\beta,h}(K_{\mathrm{d},h})^{-1}\right),\\ \text{with}\quad \Omega_2 =& (1+K_{\mathrm{I}})K_{\beta,o} + K_{\beta,h};\end{aligned} \tag{S5.37}$$

$$\begin{aligned}(K_3)^{-1} =& \frac{1}{\Omega_3}\left(K_{\beta,o}(K_{\mathrm{d},o})^{-1} + K_{\beta,h}(K_{\mathrm{d},h})^{-1} + K_{\beta,c}(K_{\mathrm{d},c})^{-1}\right),\\ \text{with}\quad \Omega_3 =& K_{\beta,o} + K_{\beta,h} + K_{\beta,c}.\end{aligned} \tag{S5.38}$$

It is therefore possible to find parameter sets for variant *ohc*-s* to reproduce three distinct apparent binding affinities in agreement with the measured ones [21] (Figure 2c).

However, for variant *ohc**-*m*, only β_3 is decoupled ($\Gamma_3^{80^\circ} = \Gamma_3^{120^\circ} = \{o, h, c\}$),

$$
\begin{aligned}
(K_3)^{-1} =& \frac{1}{\Omega_3}\left(K_{\beta,o}(K_{\mathrm{d},o})^{-1} + K_{\beta,h}(K_{\mathrm{d},h})^{-1} + K_{\beta,c}(K_{\mathrm{d},c})^{-1}\right), \\
\text{with} \quad & \Omega_3 = K_{\beta,o} + K_{\beta,h} + K_{\beta,c};
\end{aligned} \tag{S5.39}
$$

while β_1 and β_2. Nevertheless, the exact equations for K_1 and K_2 as adapted from Equation (S5.27) are too complicated to be solved analytically. We therefore attempt to obtain approximate solutions for K_1 and K_2.

To this aim, we notice that variant *ohc**-*m* includes only one less possible combinations of $(\phi, \mathcal{C}^{(1)}, \mathcal{C}^{(2)})$ compared to variant *ohc**-*w*, *i.e.*, $(120^\circ, o, c)$,

$$
\begin{aligned}
(K_1)^{-1} + (K_2)^{-1} &= (K_1^w)^{-1} + (K_2^w)^{-1} + \frac{\omega}{\Omega_{(1,2)}}\left((K_1^w)^{-1} + (K_2^w)^{-1} - (K_{\mathrm{d},o})^{-1} - (K_{\mathrm{d},c})^{-1}\right), \\
(K_1)^{-1}(K_2)^{-1} &= (K_1^w)^{-1}(K_2^w)^{-1} + \frac{\omega}{\Omega_{(1,2)}}\left((K_1^w)^{-1}(K_2^w)^{-1} - (K_{\mathrm{d},o})^{-1}(K_{\mathrm{d},c})^{-1}\right), \\
\text{with} \quad & \omega = K_{\mathrm{I}} K_{\beta,o} K_{\beta,c},
\end{aligned} \tag{S5.40}
$$

where $K_{1,2}^w$ are the apparent binding affinities of $\beta_{1,2}$ in variant *ohc**-*w*, which are given in Equations (S5.35) and (S5.36); $\Omega_{(1,2)}$ is the normalization factor given in Equation (S5.27) for variant *ohc**-*m*. Note that Equation (S5.40) means that $(K_1)^{-1}$ and $(K_2)^{-1}$ are the two roots of the quadratic equation $x^2 - Bx + C = 0$, where $B = (K_1)^{-1} + (K_2)^{-1}$ and $C = (K_1)^{-1}(K_2)^{-1}$, *i.e.*,

$$
(K_{1,2})^{-1} = \frac{1}{2}\left(B \pm \sqrt{\Delta}\right), \tag{S5.41}
$$

where $\Delta = B^2 - 4C$.

Further, we restrict our discussion to the case where $(K_{\mathrm{d},c})^{-1} \gg (K_{\mathrm{d},o})^{-1}, (K_{\mathrm{d},h})^{-1}$ and $(K_2^w)^{-1} \gg (K_1^w)^{-1}$. With these conditions, and because B^2 contain quadratic terms of $(K_2^w)^{-1}$ and $(K_{\mathrm{d},c})^{-1}$ as well as their cross-terms, it is implied that $B^2 \gg C$. Therefore,

$$
\sqrt{\Delta} = \sqrt{B^2 - 4C} = B\sqrt{1 - \frac{4C}{B^2}} \approx B(1 - \frac{1}{2}\frac{4C}{B^2}) = B - \frac{2C}{B}. \tag{S5.42}
$$

Assuming that $K_1^{-1} < K_2^{-1}$, we have

$$
K_2^{-1} = \frac{1}{2}\left(B + \sqrt{\Delta}\right) \approx B - \frac{C}{B} \approx (K_2^w)^{-1} - \frac{\omega}{\Omega_{(1,2)}}\left((K_{\mathrm{d},c})^{-1} - (K_2^w)^{-1}\right), \tag{S5.43}
$$

where $(K_{\mathrm{d},c})^{-1} - (K_2^w)^{-1} > 0$.

K_2 is expected to be close to K_2^w, thus K_2 is likely close to K_3. This explains why this variant *ohc*-m* also failed to reproduce the measured ADP binding affinities [21] (Results and Discussion).